Environmental Earth Sciences (2025) 84:82
https://doi.org/10.1007/s12665-024-12062-7

ORIGINAL ARTICLE

Effect of width-to-height ratio on the strength and behaviour of chromitite rock

Bryan Philip Watson[1] · **Tatenda John Maphosa**[1] · **Thomas Richard Stacey**[1] · **Willie Theron**[1] · **Noel Fernandes**[1]

Received: 10 July 2024 / Accepted: 21 December 2024

Abstract
The South African Bushveld Complex, Upper Group 2 (UG2) Reef pillar design has been based on a strength formula originally determined for quartzite. This formula was modified to cater for the weaker UG2 chromitite material. However, there is evidence that the pillars are stronger than predicted by the modified formula. In this study, UG2 chromitite samples were tested at a wide range of width-to-height ratios to determine the material behaviour and the relationship between strength and width-to-height ratio. Such test results on this material have not been published in the past. All testing was performed in a servo-controlled stiff testing machine (MTS 815) at a constant deformation rate of 0.08 mm/min. Specially prepared load spreader end-pieces were used to minimise any bending effects of the loading platens on the sample behaviour. The analysis showed a non-linear strengthening with increasing width-to-height ratio, best described using a power formula. A change in failure mode from pure shear to extension was observed at a width-to-height ratio of one, which has been documented previously for other materials. The change in fracture mode did not appear to affect the strength of the material. Further tests were conducted to determine the critical strain at which extension fractures initiate in chromitite. It was found that extension fracturing initiated at a critical strain of between − 2.2 mε and 3.0 mε, which was about 10 times the strain calculated by existing formulae. This new information has not been previously published for chromitite. An additional useful product of the work is an equation that can be utilised to evaluate the true uniaxial strength from samples prepared with a w/h ratio of one. Strain softening was observed on all samples up to a w/h ratio of eight. Samples with w/h ratios of three and higher were able to sustain high stresses for large strains, but almost all samples finally failed with complete loss of load. The final sudden loss of load is believed to be associated with radial cracks observed in these samples after failure.

Keywords Chromitite · Width-to-height ratio tests · Laboratory tests · Failure mechanisms · Failure criteria

Introduction

The design of pillars in the South African Bushveld Complex, Upper Group 2 (UG2) Reef, has been based on a modified version of the Hedley and Grant formula (Malan and Napier 2011). (Eq. 1). The original formula was designed on quartzite pillars (Hedley and Grant 1972) and needed adjustment to cater for the weaker UG2 chromitite material. Martin and Maybee (2000). compared six empirical pillar strength formulae for underground excavations. Each formula was developed for a separate rock type and normalised to the laboratory strength of the material. In all cases, the pillar strength was related to the width-to-height (w/h) ratio. The significant variation in the strength results between the empirical formulae suggests that a unique formula may be required for each set of geomechanical and geotechnical conditions. Recent work by Watson et al. (2021a) shows that the current, modified Hedley and Grant formula (Malan and Napier 2011) is conservative, and smaller pillars may be possible without compromising safety. The new formula developed by Watson et al. (2021a) was verified by an instrumentation site (Watson et al. 2021b), and is provided in Eq. 2. Watson et al. (2021b) showed that the new formula would achieve significant revenue creation and could impact positively on the life of the platinum mining industry. However, the formula required further verification, and a range of w/h ratio laboratory tests were done on UG2 chromitite to achieve this goal. A literature review showed that only one set of tests was done previously on this material (Ryder and

✉ Bryan Philip Watson
bryan.watson@wits.ac.za

[1] University of the Witwatersrand, Johannesburg, South Africa

Published online: 24 January 2025

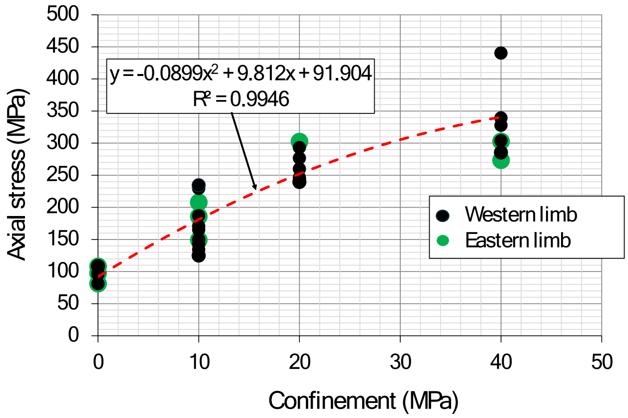

Fig. 1 Distribution of Chromitite strength values at several confining pressures, from the Western and Eastern Bushveld Complex

Jager 2002). Only three samples were tested, and no information was provided on how the tests were conducted or on the geomechanical behaviour of the rock during testing. This implies that the research described in this paper will provide new information.

$$Strength = 35\frac{w_e^{0.5}}{h_e^{0.75}}MPa \tag{1}$$

$$Strength = 67\frac{w_e^{0.67}}{h_e^{0.32}}MPa \tag{2}$$

where: w_e is the effective pillar width and h_e is the effective pillar height.

This paper provides the results of width-to-height (w/h) ratio tests conducted in a laboratory on chromitite samples. A wide range of w/h ratios was tested to determine a relationship between strength and w/h ratios ratio. In addition, fracture mode and its effect on the geomechanical results were studied. All testing was performed in a servo-controlled stiff testing machine (MTS 815) at a constant deformation rate of 0.08 mm/min following ISRM standards (Ulusay 2015).

Literature review

Since no literature on w/h ratio testing of chromitite was available, a review was conducted on the general effect of the w/h ratio on the strength and behaviour of rock specimens.

General behaviour of w/h ratio tests

Jessu and Spearing (2018) conducted w/h ratio tests on 50 mm and 54 mm diameter samples of moulded gypsum

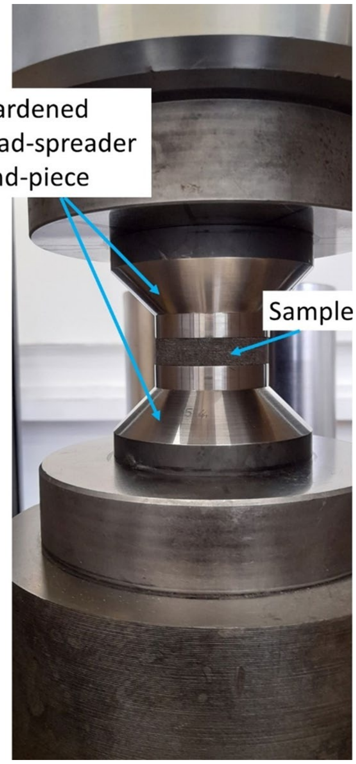

Fig. 2 Load spreader endpieces

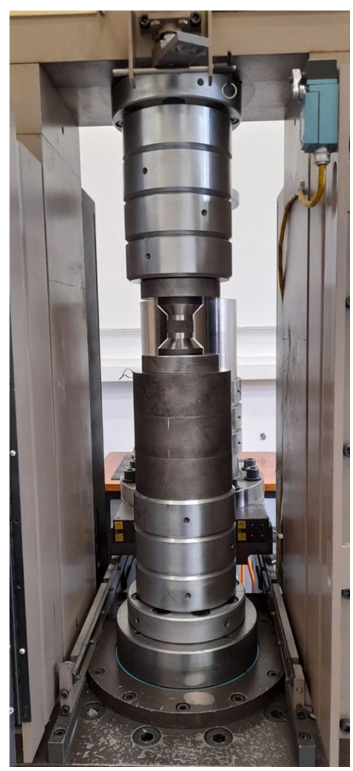

Fig. 3 Test setup

and sandstone, respectively. In that study, an almost linear relationship was observed between the w/h ratio and strength for both types of samples, within the w/h ratio range of 0.5 and 2.0. Vogler and Stacey (2016) showed a similar relationship for stabilised soil and anorthosite, but the range of w/h ratios and number of tested samples within each range was too small to be of statistical significance.

Some studies (Li et al. 2018; Darbor et al. 2018) show that for brittle rock and cementitious materials, there is a change in failure mode from shear to slabbing as sample w/h ratios are increased. A similar observation of failure mode change was made by Els and Malan (2023). However, in the latter instance, the change of failure mode was a result of changing the friction angle on the loading surface during the testing of 100 mm cement cubes. The reason for the change in failure mode is thought to be the result of exceeding a critical strain (Stacey 1981). Stacey (1981) describes how a failure that produces cracks similar to a tensile fracture, can develop under compressive stress conditions. This type of failure is strain-based (Stacey 1981) and is known as extension fracturing because it develops perpendicular to the direction of the greatest negative ("tensile") strain. Kong et al. (2021) indicated that a change in failure mode may also affect the size-strength relationship of rock samples. Wesseloo and Stacey (2016) claim that critical strains are rock-type dependent. Further testing was therefore done as part of this project, to establish a critical strain for chromitite, at which extension fracturing is likely to initiate. The effect of this change in failure mode on strength was also investigated.

Extension strain failure criterion

A simple empirical formula was produced by Stacey (1981) for extension fracture initiation and development in brittle rock. The criterion explained how an apparent "tensile" failure could occur in a compressive environment. It also explained how fractures could develop parallel to the major

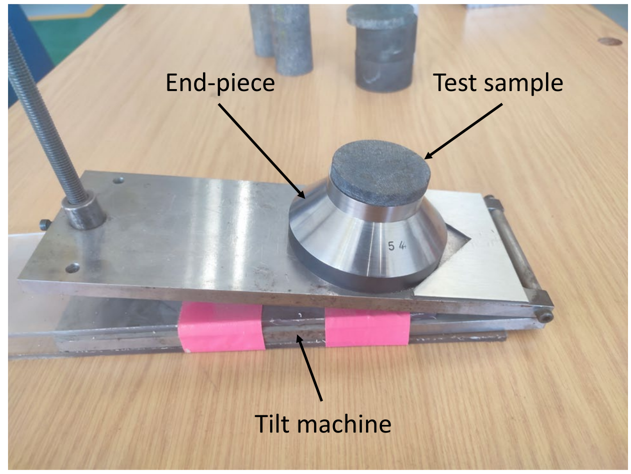

Fig. 5 Friction angle between the samples and the loading end-piece

and intermediate stresses. For a linear elastic material, Stacey (1981) proposed the following solution:

$$\varepsilon_3 = \frac{1}{E}\left[\sigma_3 - \nu\left(\sigma_1 + \sigma_2\right)\right] \tag{3}$$

where: σ_1, σ_2, and σ_3 are the principal stresses (MPa), E is Young's Modulus (MPa) and ν is the Poisson's Ratio. A fracture will initiate when:

$$\varepsilon_3 \geq \varepsilon_{cr} \tag{4}$$

where: ε_{cr} is the critical strain.

The critical strain can be calculated using the following formula (Ryder and Jager 2002):

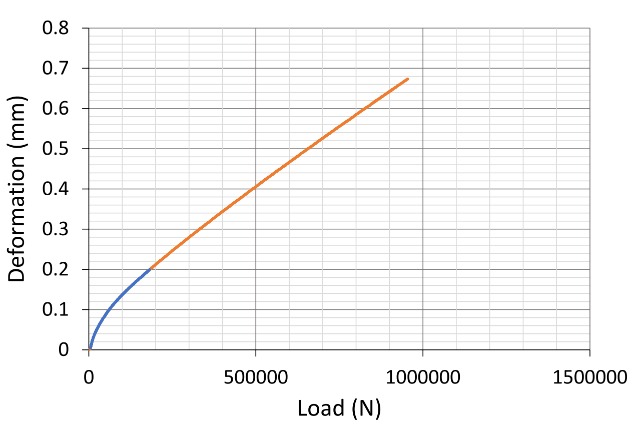

Fig. 4 Machine stiffness

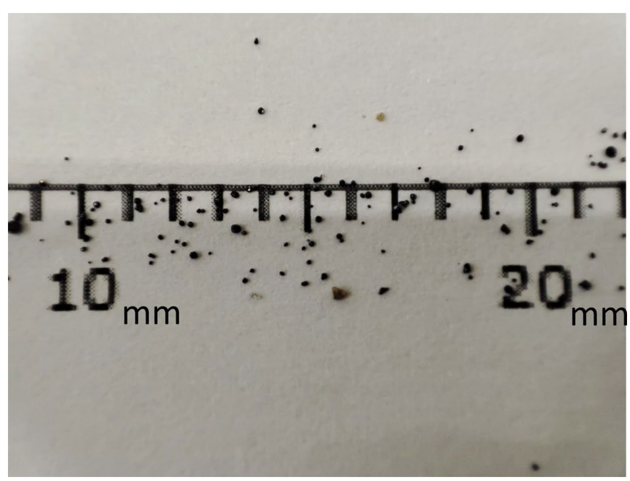

Fig. 6 Crystal size in the chromitite samples (each graduation represents 1 mm)

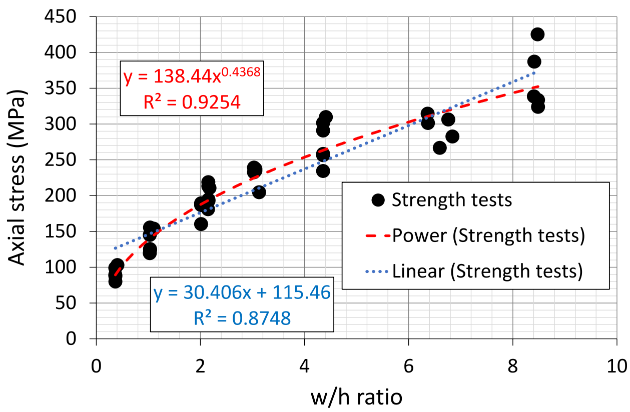

Fig. 7 Laboratory results of various w/h tests performed on chromitite. The red dashed line represents a power fit, and the blue dotted line shows a straight-line regression analysis

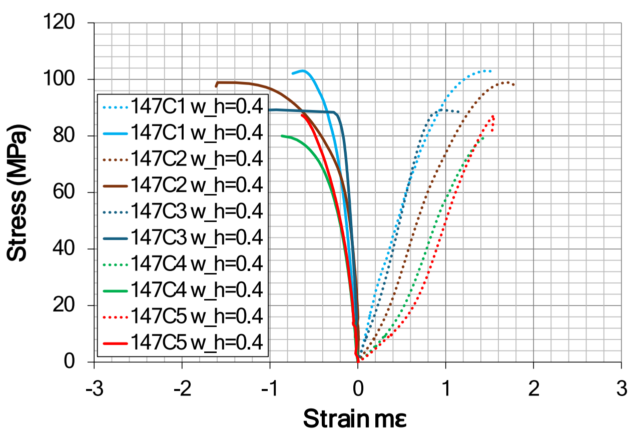

Fig. 8 UCS tests performed on strain-gauged samples of w/h = 0.37. The dotted lines represent the strains in the direction of the applied stress and the solid lines represent the strains perpendicular to the applied stress

Table 1 Results of the chromitite UCS tests

Sample No	Strength (MPa)	E (GPa)	ν (45% UCS)
147C1 w_h = 0.4	103.0	104.4	0.35
147C2 w_h = 0.4	98.9	99.0	0.30
147C3 w_h = 0.4	89.3	129.7	0.28
147C4 w_h = 0.4	80.0	87.3	0.43
147C5 w_h = 0.4	87.3	89.3	0.39
Mean	91.7	101.9	0.35
Standard dev	9.2	17.0	0.06

$$\varepsilon_{cr} = \frac{f \times UCS \times \nu}{E} \tag{5}$$

where:

Fig. 9 Shear failure observed in triaxial tests

Fig. 10 Shear failure observed in uniaxial tests (w/h ratio = 0.4)

f = 0.25 to 0.3 for fracture initiation.

f = 0.7 to 0.8 for crack damage strain.

UCS = Uniaxial Compressive Strength (MPa).

Some recent authors have disputed the calculated values for critical strain, for example, Lu et al. (2020). Such findings by previous authors created further interest in including tests that will determine the critical strain for chromitite.

Geomechanical testing of UG2 chromitite

Maphosa (2022) performed laboratory tests on UG2 chromitite samples from the western side of the Bushveld Complex. The results generally showed a small variation in strength

Fig. 11 Failure mode change with w/h ratio

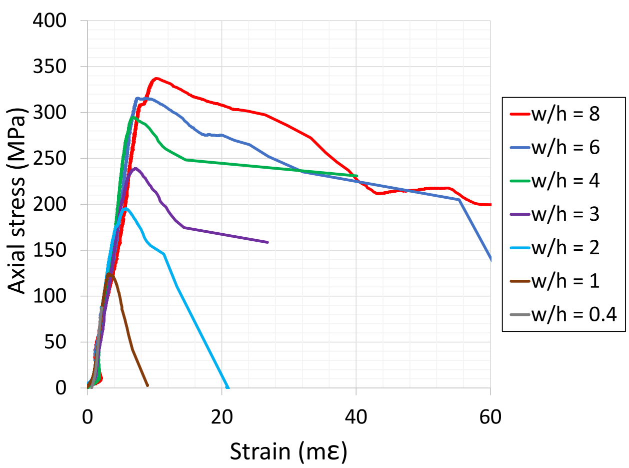

Fig. 12 Representative stress–strain curves at each w/h ratio

Table 2 Critical strains were calculated from the material properties in Table 1 using Eq. 5

Sample No	Critical strain (mε)
147C1 w_h=0.4	− 0.28
147C2 w_h=0.4	− 0.24
147C3 w_h=0.4	− 0.15
147C1 w_h=0.4	− 0.32
147C1 w_h=0.4	− 0.31

at each confinement (Fig. 1). A curved, second-order polynomial equation provided a better fit than a linear regression to the strengthening effect of confinement, suggesting non-linear behaviour of the material at fairly low confinements. Tests performed on samples from the eastern side of the Bushveld Complex were added to the original data in Fig. 1 for comparison. The results were similar to Maphosa's (2022) data set, suggesting that the chromite material is similar across the Bushveld Complex. All these tests were conducted on samples with a w/h ratio of 0.4.

Sample preparation

Samples of 54 mm diameter were prepared at various w/h ratios with loading surfaces of better than 0.02 mm flatness and parallelism as prescribed by the ISRM standards (Ulusay and Hudson 2007). Specially prepared end-piece load-spreaders (Fig. 2) were manufactured from EN30B steel that was hardened to a Rockwell hardness of HRC58 with a loading diameter surface of 54.0 mm as specified by Ulusay and Hudson (2007). The flatness and parallelism of the end-piece loading surfaces were better than the prescribed 0.02 mm (Ulusay and Hudson 2007). The test setup is shown in Fig. 3.

Transducer calibration

The testing was conducted in a servo-controlled (MTS 815) stiff testing machine. Due to the expected high loads on the squat samples, the available strain-measuring transducers were not used. Instead, axial load and deformation readings were obtained from the machine transducers. As a result, no lateral strains were made except in the cases where strain gauges were attached to the samples to determine the strains at which extension fracturing was initiated. The machine deformation measurements were influenced by the spacers and stretch in the press. These influences needed to be removed from the deformation results. This was achieved by loading the spacers and end-pieces configuration without a sample and producing a Deformation-load graph (Fig. 4). The machine deformation was subtracted from the test data using this graph.

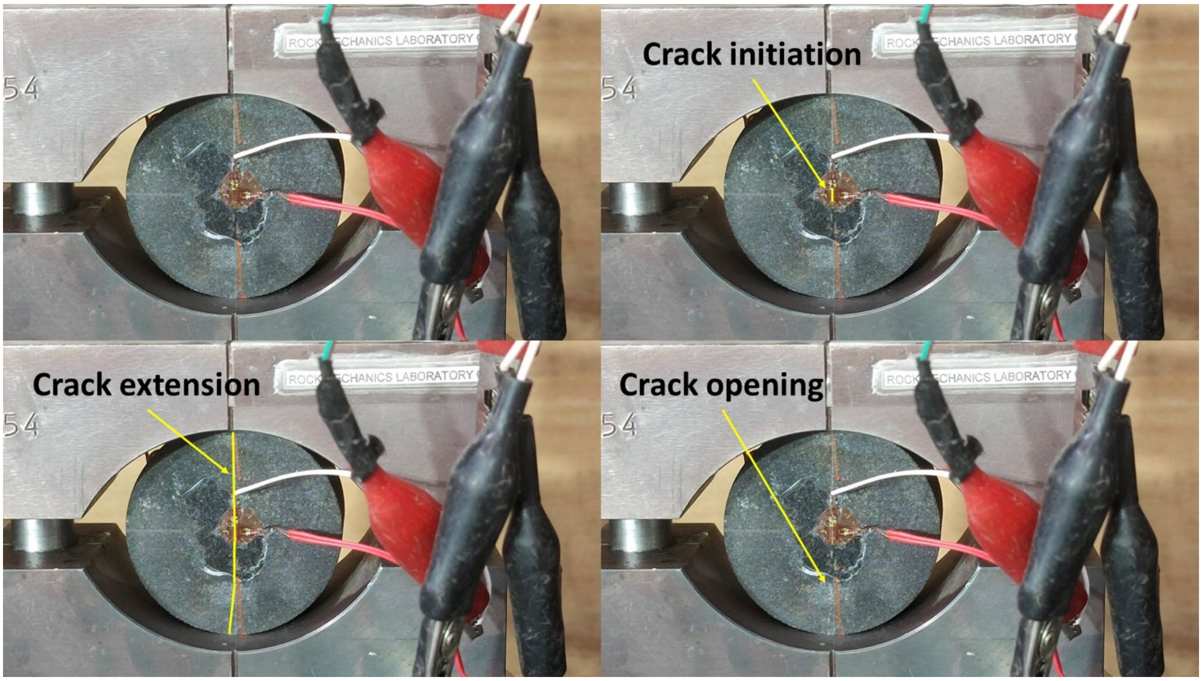

Fig. 13 Fracture propagation in a Brazilian Test using highspeed photography

Table 3 Brazilian test sample details and the critical lateral strains

Sample no	Diameter (mm)	Length (mm)	Mass (g)	Strength (MPa)	Load (kN)	Critical strain (mε)
Braz 1	53.63	26.10	225.2	4.9	10.8	Trial sample*
Braz 2	54.3	26.08	231.3	5.3	11.7	− 2.8
Braz 3	54.2	26.10	231.3	5.5	12.3	− 3.0
Braz 4	54.3	26.08	230.6	5.1	11.3	− 2.2
Average				5.2		− 2.7
Standard Dev				0.3		0.4

*No strain measurements were made

The initial loading showed non-linear behaviour, but from a load of 182 kN the calibration was linear (Fig. 4). A separate factor was determined for the initial section using a third-order polynomial fit with a correlation coefficient of 0.9989 (Appendix A). A linear regression analysis was applied to the linear region, where the correlation coefficient was 0.9949 (Appendix A).

Test procedure for the w/h ratio testing

Before testing, samples were checked for compliance with preparation standards specified by Ulusay and Hudson (2007). The parallelism and smoothness results are provided in Appendix B. Several tilt-tests were conducted on each sample to determine the average friction angle between the sample and the loading end-piece (Fig. 5). Subsequently, samples were assembled into a servo-controlled stiff testing

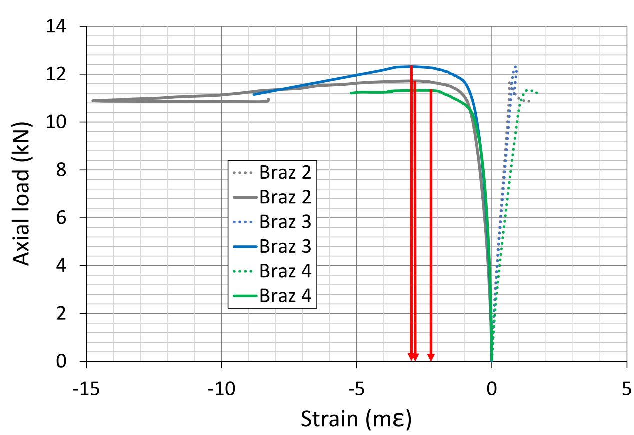

Fig. 14 Load as a function of strain parallel (dotted lines) and perpendicular (solid lines) to the loading direction. The tensile strains at which fracture development was initiated in the Brazilian tensile tests are shown by the red arrows

Table 4 Critical strain results for cylindrical UCS samples with w/h of 1.1

Sample no	Diameter (mm)	Length (mm)	Critical strain (mε)	Stress at critical strain (MPa)
C1-0.21mε	54.1	49.00	Not achieved*	
C1-0.28 mε	54.1	49.00	Not achieved*	
C1-2.92 mε	54.1	49.00	− 2.92	175.9
C2	54.2	49.00	Gauge damaged	
C3	54.2	49.00	− 1.69	151.0
C4	54.2	49.00	− 2.12	153.3
Average			− 2.2	160.1
Std. dev			0.6	13.8

*The test was stopped at various strains to determine if extension fracturing had occurred

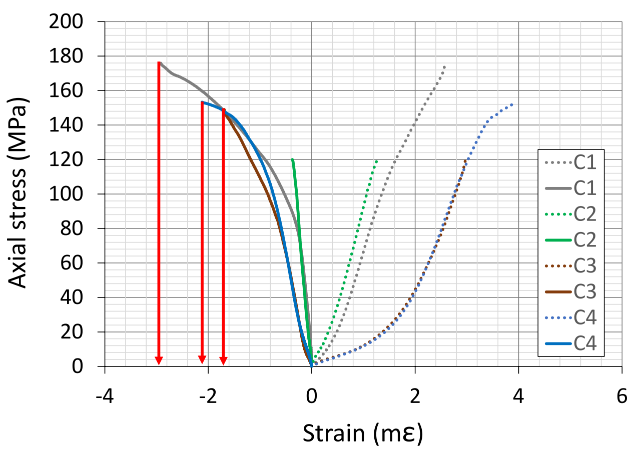

Fig. 15 Stress–strain results for UCS samples of w/h = 1, showing axial strains (dotted lines) and radial strains (solid lines) as a function of axial stress. The radial strains at which extension fractures are initiated are shown by the red arrows

machine (MTS 815) as shown in Fig. 2 and Fig. 3. The samples were tested at a constant deformation rate of 0.08 mm/min following ISRM standards (Ulusay 2015).

Five samples were tested at each of seven different w/h ratios, in line with the ISRM standards for minimum numbers of tested samples (Ulusay and Hudson 2007). In addition, the minimum number of grains (crystals) between the loading platens was never less than 20 through the sample thickness. Ulusay and Hudson (2007) suggest that the ratio of sample size to grain size should not be smaller than ten. The typical range of crystal sizes is shown in Fig. 6, where each graduation between 10 and 20 mm is 1 mm.

Test results

The test results are shown in Fig. 7 and the details are provided in Appendix B. Individual stress–strain curves are provided in Appendix C. Normal UCS tests with strain gauges were performed on samples with a w/h ratio of 0.4 (slender samples). The geomechanical results are provided in Fig. 8 and the material properties are shown in Table 1. Note that the range in strength shown in Fig. 8 is similar to the UCS tests shown in Fig. 1 and the elastic constants are also similar. The results in Fig. 7 show that the w/h strengthening effects in the laboratory data are better represented by a power, rather than, a linear formula. Note that there was a change in failure mode from pure shear to extension with shear between w/h ratios of 0.4 and 1.1. The literature

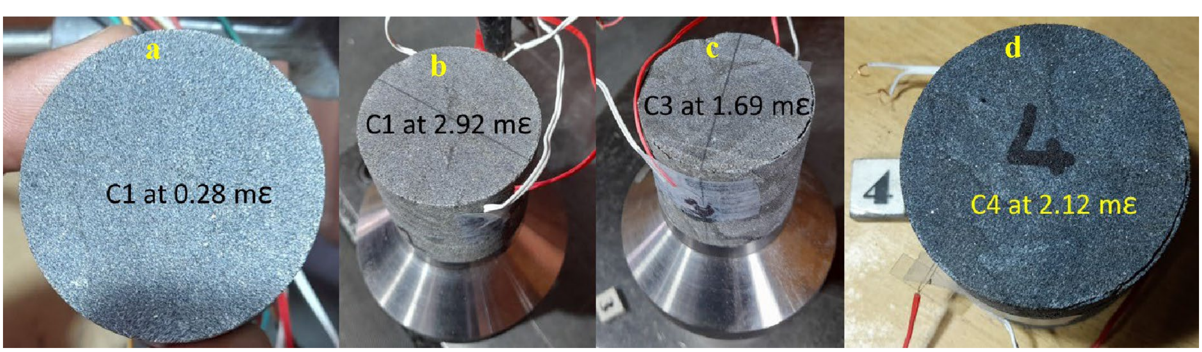

Fig. 16 Photographs of the w/h = 1 samples, showing the fracture condition at various lateral strains

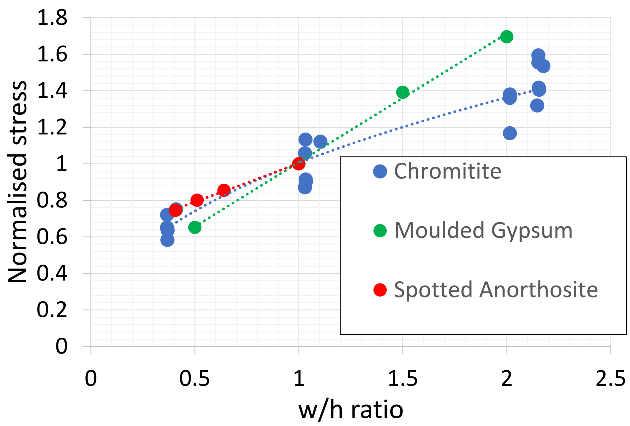

Fig. 17 Comparison between the normalised strengthening effects of w/h ratio on chromitite, moulded gypsum and spotted anorthosite

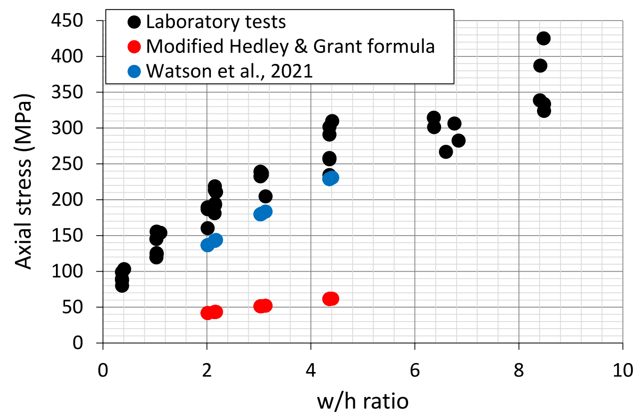

Fig. 18 Laboratory results of various w/h ratio tests performed on chromitite and the Modified Hedley and Grant formula for pillar strength calculations on the UG2 chromitite pillars

review suggests that the behaviour of the latter ratio may have been influenced by the confining effects of the end pieces and the magnitude of the critical lateral strain for chromitite. Extension failure was not observed on the slender samples, either during uniaxial or triaxial testing, up to a confinement of 40 MPa.

Observed failure modes in the laboratory tests

The failure mode for the triaxial tests, from confinements of 10 MPa up to 40 MPa, was a single shear plane as shown in Fig. 9 (Maphosa 2022). Most uniaxial tests performed on slender samples failed with a double shear plane (Fig. 10), forming cones adjacent to the loading platens (Carpede 2023). At a w/h ratio of 1:1, extension fracturing was first observed on the outer edges, just before failure. The final failure appears to have been on double-shear planes through the undamaged centre portion of the sample (Fig. 11). Cones were also observed in the samples with a w/h ratio of one (Fig. 11). A change in failure mode at a w/h ratio of one was also observed by Li et al. (2011) on another material. Extension fracturing became prominent in the samples with a w/h ratio of two, and there was also evidence of multiple shear planes, which is believed to be a secondary formation at the time of final failure (Fig. 10). From a w/h ratio of three, extension fracturing became much more dominant with concentric rings of extension failure as failure progressed to the centre (Fig. 11). Load loss was not observed during the development of extension fractures. Zhao et al. (2022) observed an increase in plastic deformation between the yield and failure with w/h ratio on rectangular-shaped granite tests. Such behaviour was not obvious in the chromitite tests (Fig. 12).

Multiple shear failure planes and radial extension cracks were observed in the damaged chromitite material. A general reduction in extension fracturing was observed at the centre of the specimens with a w/h ratio above three, and at a w/h ratio of about eight, a significant central core developed (Fig. 11), apparently without extension fractures, but friable and not as strong as the pretested sample.

Critical strain for extension fracture development

The critical strains at which extension strain damage should be visible were determined using Eq. (5) with "f" set to 0.8 and using the material properties provided in Table 1. The results are shown in Table 2.

Li and Wong (2013) suggested that the extension strain criterion may be suitable for explaining crack initiation and propagation in a Brazilian indirect tensile test. A verification process was therefore performed using strain-gauged Brazilians and axially loaded samples with a w/h ratio of 1.1. Samples were carefully prepared from 54 mm diameter chromitite cores to ISRM standards for Brazilian Tensile testing (Ulusay and Hudson 2007). The two flat Brazilian test surfaces were polished to better than 0.02 mm of flatness and parallelism. Vertical and horizontal strain gauges of 3 mm in length were attached to the centre of both flat surfaces (Fig. 13). Testing was done in a jig and the strength calculations were made as per ISRM standards (Fig. 13) and the strain at the centre of the disc was monitored in both the axial and lateral directions. A loading rate of 0.3 mm per minute was used so that failure took place in about 1.4 min (ISRM 1978). The results are shown in Table 3 and Fig. 14. The critical strains were taken as the lateral strain where crack development was initiated.

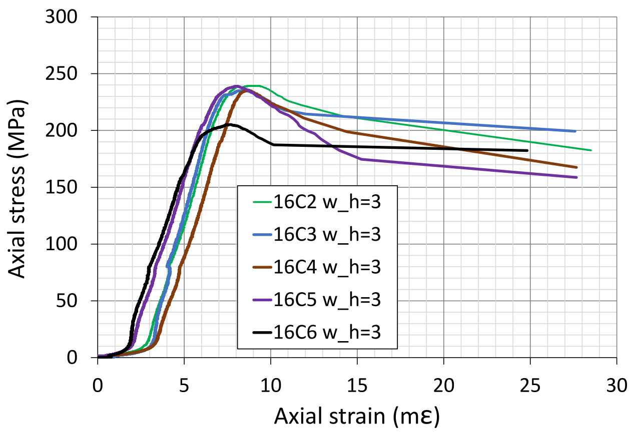

Fig. 19 Stress/strain curves for samples of w/h = 3

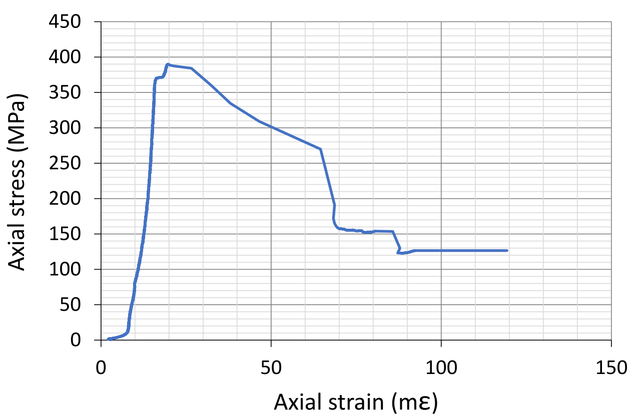

Fig. 20 Stress/strain curve for Sample 6C4 (w/h = 8.4)

The Brazilian tests suggested a critical strain of about 10 times the calculated strain. However, loading in the Brazilian tests took place over an arc which is different to the original application of the criterion (Stacey 1981). Further tests were conducted on strain-gauged UCS samples with a w/h ratio of 1.1. The results of this testing are shown in Table 4 and Fig. 15. Critical strains were where the radial strain exceeded the critical strain. The first sample was tested to the calculated critical strain levels initially, but there were no obvious signs of fracturing (Table 4). Subsequently, the samples were loaded until the strain gauges became unstable. The point at which the strain gauge readings became unstable was considered to represent the critical strain (Table 4). In these samples, the critical strain appears to have occurred just before failure.

Test C1 was stopped at the critical strains predicted by Eq. (5), but no signs of extension fracturing were observed at these radial strains (Fig. 16a). Finally, the test was stopped at a radial strain of 2.92 mε and evidence of extension strain was observed (Fig. 16b) This sample was unusually strong and appears to have provided an unusually high critical strain. However, the critical strains shown by Tests C3 and C4 were similar to the values shown by the Brazilian tests (Fig. 16c and d).

Discussion of results

The test laboratory provides a controlled environment where factors such as the effects of w/h ratio on strength can be determined. However, the effects of flaws are not properly considered in 50 mm diameter samples (Hoek and Brown 1980). The results are therefore likely to be stronger than the rock mass. In addition, the effects of the foundation materials were not considered in the laboratory tests performed in this project. However, valuable information on the general behaviour of chromitite was obtained. Bieniawski and van Heerden (1975); Ryder and Ozbay (1990); York and Canbulat (1998) and Watson et al. (2010) found a linear relationship between w/h ratio and strength for other hard-rock materials. Such behaviour was also observed by Jessu and Spearing (2018) and Vogler and Stacey (2016) in their laboratory tests performed on moulded gypsum and spotted anorthosite, respectively. The results of their investigation are compared to the chromitite tests in Fig. 17, by normalising to a w/h ratio of one.

In this study, a curved fit best described the tests performed on chromitite (Fig. 7 and 17). The results correspond to the nonlinear behaviour in the triaxial tests performed by Maphosa (2022) at fairly low confinements. The behaviour of the rock under a range of w/h ratios has implications for the type of formula that should be used to describe pillar strength. The test results in this project clearly show that a power formula best describes the strengthening effects of the w/h ratio on strength for chromitite (Fig. 7). This finding agrees with the results recorded by Watson et al. (2021a) for chromitite pillars.

The currently used Modified Hedley and Grant (Malan and Napier 2011) and the Watson et al. (2021a) formulae are plotted with the laboratory tests in Fig. 18. There is a significant difference between the strength predicted by the Modified Hedley and Grant formula (Malan and Napier 2011) and the laboratory tests. However, there is a much closer match when these tests are compared to the Watson et al. (2021a) formula. The underground pillars represented by Watson et al. (2021a) are weaker than the laboratory test, as expected due to the size of the laboratory test samples. The Watson et al. (2021a) formula for pillar design allows for smaller pillars and greater extraction ratios than the current Modified Hedley and Grant formula (Malan and Napier 2011). It should be noted that the samples at a w/h ratio of eight may not give the actual strength of the rock due to their thickness.

The results of the laboratory tests suggest that the loading platens provide a significant confining effect on the specimen, even under relatively low contact friction angles (Appendix B). The confinement effects can be observed in the large increase in strength between w/h ratios of 0.4 and 1.1. The excellent power formula fit to the data in Fig. 7, suggests that the equation given in the figure may be used to determine the material UCS from smaller samples. The equation may be useful when borehole core lengths are too small for normal UCS tests. Should it be only possible to prepare chromitite samples with a w/h ratio of one, the following formula may be used to determine UCS:

$$UCS = \sigma_{c1} \times 0.4^{0.347} \quad (6)$$

where: σ_{c1} is the strength of a sample with w/h = 1.

York & Canbulat (1998) also reported low contact friction angles for their laboratory tests on pyroxenite samples. However, the contact surfaces underground are expected to be about 30° (Ryder and Jager 2002). The low friction angle is likely to reduce the strength of the laboratory samples and encourage early extension fracturing (Els and Malan 2023). Owing to the steel platens in the laboratory tests, fracturing was not allowed to develop into the foundation (as would be the situation for underground pillars). This condition may have had an opposite, strengthening effect on the laboratory results (Watson et al. 2009). Further testing is thus required using rock platens with the same material properties and contact surface friction angles as the pillar foundation materials. Such rock platens will need to be confined with metal rings to avoid the development of radial fractures or splitting of the platens. In this way, damage will be permitted to propagate into the foundation materials. Surface conditions will, however, need to be roughened to account for the likely contact friction underground.

All the samples with a w/h ratio of two and less failed with complete load loss. From a w/h ratio of 3.0 the samples were able to maintain a high strength beyond failure for a considerable axial strain (Fig. 19). However, in almost all cases, there was a slow deterioration in the ability to carry the load, suggesting that some fracturing or extending of fractures was taking place in the samples. A complete load loss was observed in most samples at all w/h ratios. The load loss appears to have coincided with the development of radial cracks, which can be observed in Fig. 11. These radial cracks are suspected to have facilitated the final stress drop to zero. Only one sample was semi-stable, and a residual strength was achieved (Fig. 20). It is not clear why this sample was more stable than the others at high strains. The residual strength was high on this sample but lower than expected for a w/h ratio of 8.4. Work done by Watson et al. (2010) suggests that the residual strength of a high w/h ratio pillar is dominated by the damaged foundation, which, in this case, was prohibited by the steel platens in the laboratory tests.

Several authors have reported a change in failure mode from shear to extension at a w/h ratio of one for a variety of rock types (Li et al. 2018, 2011; Darbor et al. 2018). A similar finding was made for the tests conducted for this research project. However, close observations of the samples suggested extension fractures on the outer perimeter of the sample and shear fractures developed on the inner core of the samples at a w/h ratio of 1.1. At higher w/h ratios shear fractures appear to have developed as a secondary failure mechanism within the slabs formed by extension fracturing (Fig. 11). Tests done by Els and Malan (2023) showed a change in failure mode when changing the contact friction angle on samples with the same w/h ratio. These results suggest that the fracture patterns and density of fracturing may change at higher friction angles. It is not clear if the change in fracture mode affected the w/h strengthening effect shown in Fig. 7. However, no obvious load loss or increase in plastic deformation is shown by the stress–strain curves in Fig. 12. It should be noted, however, that similar fracturing is observed underground in the sidewalls of highly stressed pillars, where w/h ratios are greater than one. The theory of extension failure suggests that a fracture develops parallel to the major and intermediate stresses when the negative strain in the direction of the minor stress exceeds a critical value (Stacey 1981). In pillars, such fracturing will occur parallel to the pillar sidewalls because the stresses perpendicular to the sidewalls are zero or small near the pillar edge. Importantly, the tests show that the presence of extension fractures does not mean the sample has failed. This finding can also be applied to pillars underground.

Work done by Li and Wong (2013) suggested that the extension strain failure criterion may be able to explain crack initiation and propagation in a Brazilian test. However, the strains measured in the Brazilian tests on chromite did not show any damage at the calculated critical strains. Interestingly, the critical strains measured on the axially loaded samples with a w/h ratio of one were similar to those measured on the Brazilian tests. These results suggest that under the described loading conditions imposed on the samples, the critical strain at which extension fractures developed was about ten times the calculated strains. The findings suggest that further research is required on the current criterion for extension strain fracture development (Eq. 5). The measured strains compare favourably with the calculated critical strains if the factor (*f*) in the equation is increased by a multiple of 10. The difference in the calculated and measured strains may be due to a different loading path to what was used when the original criterion was developed (Ryder and Jager 2002).

Conclusions and recommendations

The work done by Martin and Maybee (2000) shows a wide variation in strength formula developed for different rock types. The results suggest a unique empirical formula for each rock type and geotechnical setting. Watson et al. (2021a) developed a formula for the UG2 chromitite reef in South Africa and found that it predicted a much stronger pillar than the traditionally used Modified Hedley and Grant formula (Malan and Napier 2011). This finding was authenticated by an instrumentation site (Watson et al. 2021b), but laboratory tests were needed to validate the formula further. Watson et al. (2021b) showed a substantial impact on revenue and the life of the platinum mining industry was possible by using this formula. The research reported in this paper is the results of w/h ratio tests performed on UG2 chromitite in a laboratory.

The strengthening effects of the w/h ratio on chromitite have not been previously determined in a test laboratory. The strength profile with the w/h ratio is shown by the laboratory test results to be best described by a power formula. This result agrees with the findings of the underground investigations for UG2 chromitite pillars (Watson et al. 2021a). Tests performed by other authors on different materials have shown a linear relationship between strength and w/h ratio. The power formula fit to the test data in Fig. 7 is remarkably good, suggesting that it could be used to determine the UCS of chromitite when specimens have a w/h ratio of one. A suitable formula has been provided in the paper.

Changes in the failure mode of chromitite core samples were observed at a w/h ratio of one, in line with the findings of similar tests on other rock materials and observations on underground pillars. An important finding was that the formula for determining the critical strain for extension fracturing underestimated this strain by about a factor of 10 for UG2 chromitite.

The development of the extension fractures, parallel to the direction of loading, did not appear to result in a measurable load loss or increase in plastic deformation (Fig. 12). The observed extension fracturing in the laboratory also occurs on highly stressed pillars underground. Importantly, the results show that the presence of extension fractures does not mean sample failure. This finding can also be applied to pillars underground.

A significant effect of the loading surfaces on strength was observed, particularly at the lower w/h ratios. This effect was observed even when the friction angle between the loading surfaces was relatively small. Radial cracks were observed in the samples from a w/h ratio of 3.0. These radial cracks are suspected to have facilitated the final stress drop to zero. It is not known if this fracturing occurs in underground pillars, where fracturing is allowed to penetrate the loading surfaces and the contact friction angle between a pillar and its foundations is higher than those of the test samples.

The test results suggest the Watson et al. (2021a) strength formula for UG2 chromitite pillars may be correct. A stronger pillar implies that smaller pillars can be cut with a corresponding increase in extraction ratio. The higher extraction ratio can provide additional profit and increase the life of mines without compromising safety.

It is recommended that further testing of chromitite w/h ratio samples be done using appropriate rock platens of the same material as the pillar foundations. Such tests will allow for fractures to develop into the loading platens.

The effects of sample size on strength need to be established for chromitite. A range of sample sizes at a w/h ratio of one should be tested in a laboratory setting to determine the effects of volume. These tests will be used to establish the true “k-value” for chromitite in the power formula for pillar strength.

The tests performed in this project have provided a valuable contribution to knowledge and similar w/h ratio studies are recommended for other rock types to establish possible trends. The research shows that further work is required on the current criterion for extension strain fracture development (Eq. 5).

Appendix A

The stiffness calibrations of the machine used in the tests are provided in Figs. 21 and 22.

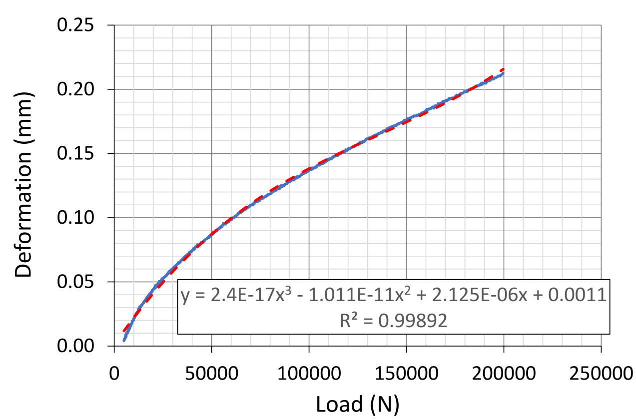

Fig. 21 Calibration used up to 182 kN

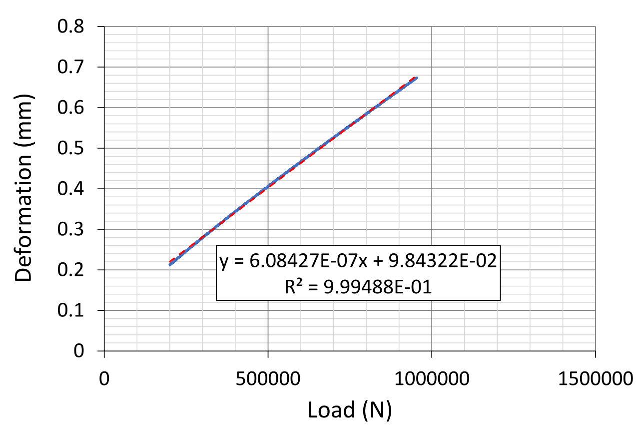

Fig. 22 Calibration used from 182 kN

Appendix B

The laboratory w/h ratio test data is provided in Table 5. The test numbering system included the planned length of the sample, material type (C=Chromitite), sample number and the planned w/h ratio.

Table 5 Laboratory test results on chromitite

Test number	Parallelism (mm)	Friction angle (°)	Diameter (mm)	Length (mm)	w/h ratio	Strength (MPa)
147C1 w_h=0.4	0.020		46.8	115.0	0.41	103.0
147C2 w_h=0.4	0.026		54.1	147.60	0.37	98.9
147C3 w_h=0.4	0.026		54.0	147.40	0.37	89.3
147C4 w_h=0.4	0.026		54.2	147.20	0.37	80.0
147C5 w_h=0.4	0.026		54.3	147.10	0.37	87.3
54C1 w_h=1	0.015	12	54.4	52.65	1.03	125.4
54C2 w_h=1	0.010	10	54.2	52.65	1.03	119.5
54C3 w_h=1	0.005	13	54.0	52.40	1.03	145.1
54C4 w_h=1	0.005	13	54.2	52.40	1.03	124.0
54C5 w_h=1	0.005	13	54.1	49.00	1.10	153.8
54C6 w_h=1	0.005	13	54.1	52.40	1.03	155.4
25A0.5 w_h=2			54.2	26.90	2.01	189.3
25B05 w_h=2		20	54.2	26.90	2.01	160.2
25C05 w_h=2		20	54.2	26.90	2.01	186.7
25C1 w_h=2	0.05		53.7	24.95	2.15	213.3
25C2 w_h=2	0.03	18	54.3	24.95	2.18	210.6
25C3 w_h=2	0.03	16	53.8	24.95	2.15	194.4
25C4 w_h=2	0.01	16	53.7	24.95	2.15	218.7
25C5 w_h=2	0.02	17	53.6	24.95	2.15	181.0
25C6 w_h=2	0.03	13	53.8	24.95	2.16	192.8
16C2 w_h=3	0.01	14	53.8	17.75	3.03	239.1
16C3 w_h=3	0.015	14	53.8	17.75	3.03	232.5
16C4 w_h=3	0.025	13	53.8	17.60	3.06	234.7
16C5 w_h=3	0.020	11	53.8	17.60	3.06	237.3
16C6 w_h=3	0.01	14	53.8	17.20	3.13	204.6
12C1 w_h=4	0.02	14	53.8	12.35	4.36	301.5
12C2 w_h=4	0.01	14	53.8	12.35	4.36	258.2
12C3 w_h=4	0.01	15	53.8	12.35	4.36	290.8
12C4 w_h=4	0.03	12	53.8	12.35	4.36	234.3
12C5 w_h=4	0.04	14	53.8	12.35	4.36	256.4
12C6 w_h=4	0.005	13	53.8	12.20	4.41	309.7
8C1 w_h=6	0.005	12	54.1	8.20	6.60	266.7
8C2 w_h=6	0.005	14	54.2	8.50	6.37	301.3
8C3 w_h=6	0.005	14	54.1	8.50	6.36	314.4
8C4 w_h=6	0.005	14	54.1	8.00	6.76	306.2
8C5 w_h=6	0.005	13	54.0	7.90	6.84	282.5
6C1 w_h=8	0.006	12	54.3	6.40	8.48	323.9
6C2 w_h=8	0.02	17	53.8	6.40	8.41	338.6
6C3 w_h=8	0.01	15	53.8	6.40	8.41	387.0
6C4 w_h=8	0.005	12	54.2	6.40	8.48	425.1
6C5 w_h=8	0.015	12	54.3	6.40	8.48	333.5
6C6 w_h=8	0.01	12	54.3	6.40	8.48	336.3

Appendix C

The individual stress/strain curves are provided in Figs. 23, 24, 25, 26, 27, 28, 29.

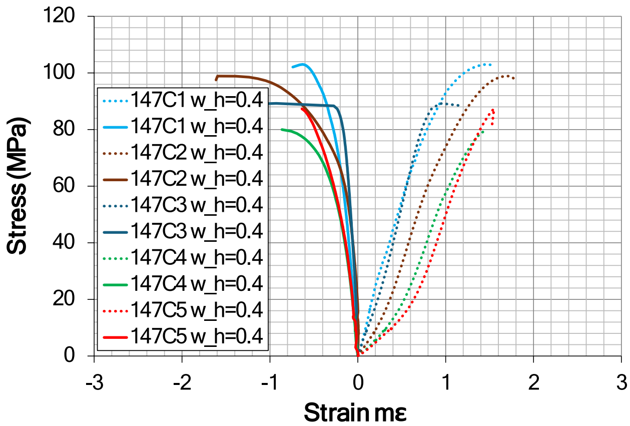

Fig. 23 Uniaxial compressive tests with strain gauges (w/h ratio = 0.37). The dotted lines represent the strains in the direction of the applied stress and the solid lines represent the strains perpendicular to the applied stress

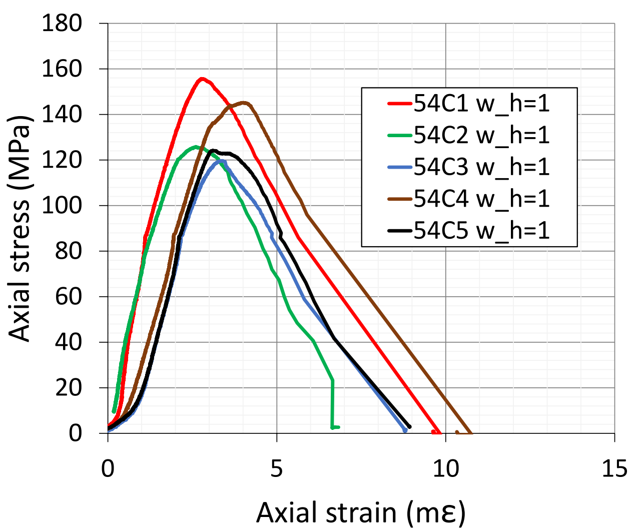

Fig.24 Uniaxial compressive tests with machine transducers (w/h ratio = 1). Only axial strains were measured

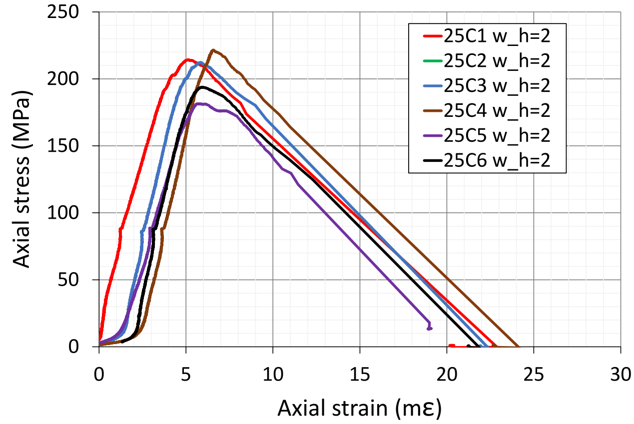

Fig. 25 Uniaxial compressive tests with machine transducers (w/h ratio = 2). Only axial strains were measured

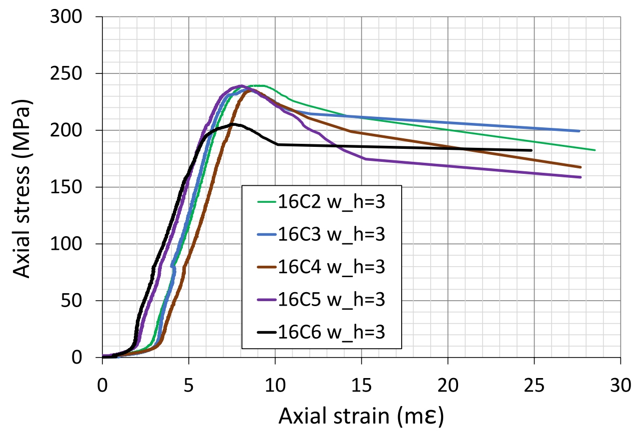

Fig. 26 Uniaxial compressive tests with machine transducers (w/h ratio = 3). Only axial strains were measured

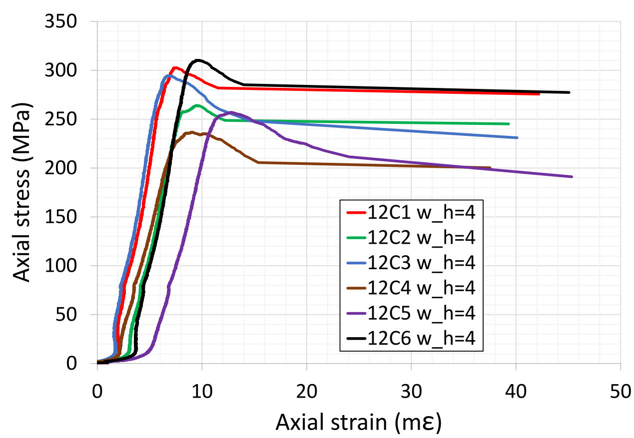

Fig. 27 Uniaxial compressive tests with machine transducers (w/h ratio = 4). Only axial strains were measured

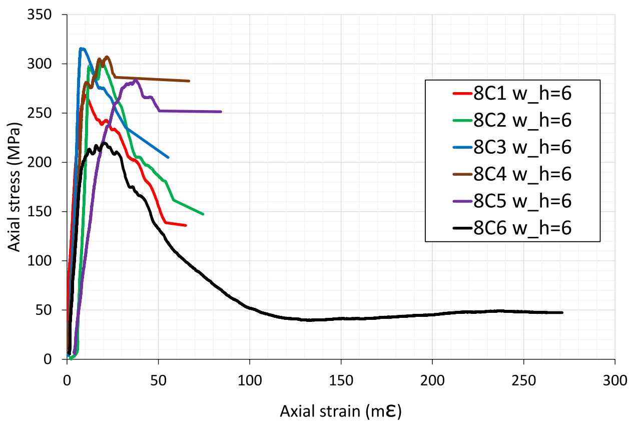

Fig. 28 Uniaxial compressive tests with machine transducers (w/h ratio = 6). Only axial strains were measured

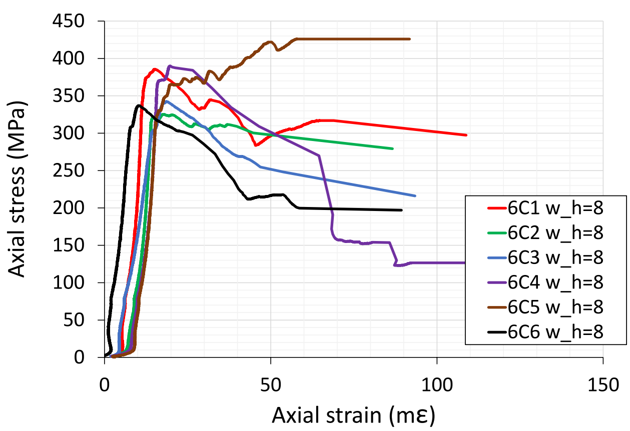

Fig. 29 Uniaxial compressive tests with machine transducers (w/h ratio = 8). Only axial strains were measured

Acknowledgements The Rock Engineering Department of Booysendal Platinum Mine is acknowledged for providing suitable cores for geomechanical testing. The University of the Witwatersrand laboratory staff are thanked for the preparation of the apparatus and test samples. In particular, Mr Morgan is acknowledged for his accurate manufacture of load spreader end-pieces and Mr Carpede is thanked for the high-quality preparation of the chromitite samples.

Author contribution All authors contributed to the study's conception and design. Material preparation, data collection and analysis were performed by Bryan Philip Watson, Tatenda John Maphosa and Noel Fernandes. The first draft of the manuscript was written by Bryan Philip Watson under guidance given by Thomas Richard Stacey. All authors commented on previous versions of the manuscript. All authors read and approved the final manuscript.

Funding Open access funding provided by University of the Witwatersrand. This work was supported by Northam Platinum LTD ($ 4,400 USD), and the University of the Witwatersrand paid for the purchase and manufacturing of the required load-spreader end pieces.

Data availability No datasets were generated or analysed during the current study.

Declarations

Conflict of interest The authors declare no conflict interests.

Generative AI and AI-assisted technologies in the writing process During the preparation of this work, the authors used BING to find suitable publications. After using this service, the authors reviewed and edited the content.

References

Bieniawski ZT, van Heerden WL (1975) The significance of in situ tests on large rock specimens. Int J Rock Mechan Min Sci Geomechan 12:55–73. https://doi.org/10.1016/0148-9062(75)90004-2

Carpede A (2023) Personel Communication. Johannesburg, SARES

Darbor M, Faramarzi L, Sharifzadeh M (2018) Size-dependent compressive strength properties of hard rocks and rock-like cementitious brittle materials. Geosyst Eng 22(4):179–184. https://doi.org/10.1080/12269328.2018.1431961

Els RP, Malan DF (2023) Calibration of the limit equilibrium pillar failure model using physical models. J Southern Afr Inst Min Metallurgy 123(5):253–264. https://doi.org/10.17159/2411-9717/2655/2023

Hedley DGF, Grant F (1972) Stope pillar design for the Elliot Lake uranium mines. Bull Can Inst Min Metall 65:37–55

Hoek E, Brown ET (1980) Underground excavations in rock. Institution of Mining and Metallurgy, New York

ISRM (1978) Suggested methods for determining tensile strength of rock materials part 2: suggested method for determining indirect tensile strength by the brazil test. Int J Rock Mech Min Sci 15:99–103. https://doi.org/10.1016/0148-9062(78)90003-7

Jessu KV, Spearing AJS (2018) Effect of dip on pillar strength. J Southern Afr Inst Min Metallurgy 118(07):765–776. https://doi.org/10.17159/2411-9717/2018/v118n7a10

Kong X, Liu Q, Lu H (2021) Effects of rock specimen size on mechanical properties in laboratory testing. J Geotechn Geoenviron Eng 147(5):753–769. https://doi.org/10.1061/(ASCE)GT.1943-5606.0002478

Li D, Wong LNY (2013) The Brazilian disc test for rock mechanics applications. Rock Mech Rock Eng 46:269–282. https://doi.org/10.1007/s00603-012-0257-7

Li D, Li CC, Li X (2011) Influence of sample height-width ratios on failure mode for rectangular prism samples of hard rock loaded in uniaxial compression. Rock Mech Rock Eng 44:253–269. https://doi.org/10.1007/s00603-010-0127-0

Li X, Feng F, Li D, Du K, Ranjith PG, Rostami J (2018) Failure characteristics of granite influenced by sample height-to-width ratios and intermediate principal stress under true-triaxial unloading conditions. Rock Mech Rock Eng 51(5):1321–1340. https://doi.org/10.1007/s00603-018-1414-4

Lu A, Zhang N, Zeng G (2020) An extension failure criterion for brittle rock. Adv Civil Eng 2020:1–12. https://doi.org/10.1155/2020/8891248

Malan DF, Napier JAL (2011) The design of stable pillars in the bushveld complex mines: A problem solved? J South Afr Inst Min Metall 111:821–836

Maphosa TJ (2022) *Optimum depth for the introduction of crush pillars at impala platinum mine.* MSc dissertation, School of Mining Engineering, University of Witwatersrand, Johannesburg, RSA.

Martin CD, Maybe WG (2000) The strength of hard-rock pillars. Int J Rock Mech Min Sci 37:1239–1246. https://doi.org/10.1016/S1365-1609(00)00032-0

Ryder JA, Ozbay MU (1990) *A methodology for designing pillar layouts for shallow mining.* ISRM Symposium - Static and Dynamic Considerations in Rock Engineering, Swaziland, September: **1990:** 030

Ryder JA, Jager AJ (2002) A textbook on Rock mechanics for Tabular Hard Rock Mines. SIMRAC, Johannesburg

Stacey TR (1981) A simple extension strain criterion for fracture of brittle rock. Int J Rock Mecha Min Sci Geomechan 18:469–474

Ulusay R (2015) Suggested methods for rock failure criteria: general introduction. In: Ulusay R (ed) The ISRM Suggested Methods for Rock Characterization, Testing and Monitoring: 2007–2014. Springer, Cham, pp 223–223

Ulusay R, Hudson JA (2007) The complete ISRM suggested methods for rock characterization, testing and monitoring: 1974–2006. ISRM Turkish Group, Ankara

Vogler UWOL, Stacey TR (2016) The influence of test specimen geometry on the laboratory-determined Class II characteristics of rocks. J Southern Afr Inst Min Metallurgy 116:987–1000. https://doi.org/10.17159/2411-9717/2016/v116n11a1

Watson BP, Kuijpers JS, Miovsky P (2009) In situ measurements of Merensky pillar behaviour at Impala Platinum. J South Afr Inst Min Metall 109(9):745–754

Watson BP, Kuijpers JS, Stacey TR (2010) Design of Merensky Reef crush pillars. J South Afr Inst Min Metall 110(10):581–591

Watson BP, Lamos RA, Roberts DP (2021a) PlatMine pillar strength formula for the UG2 Reef. J Southern Afr Inst Min Metallurgy 121(8):437–448. https://doi.org/10.17159/2411-9717/1387/2021

Watson BP, Theron W, Fernandes N, Kekana WO, Mahlangu MP, Betz G, Carpede A (2021b) UG2 pillar strength: verification of the platmine formula. J Southern Afr Inst Min Metallurgy 121(8):449–456. https://doi.org/10.17159/2411-9717/1491/2021

Wesseloo J, Stacey TR (2016) A reconsideration of the extension strain criterion for fracture and failure of rock. Rock Mech Rock Eng 49:4667–4680. https://doi.org/10.1007/s00603-016-1059-0

York G, Canbulat I (1998) The scale effect, critical rock mass strength and pillar system design. J Southern Afr Inst Min Metallurgy 98(1):23–45

Zhao Y, Huang L, Li X, Li C, Chen Z, Cao Z (2022) Failure modes and slabbing mechanisms of hard rock with different height-to-width ratios under uniaxial compression. Nonferrous Metals Soc China 33:3697–3712. https://doi.org/10.1016/S1003-6326(22)66050-3